

1 **Creep on seismogenic faults: Insights from analogue earthquake**  
2 **experiments**

3 Matthias Rosenau\*, Michael Rudolf and Onno Oncken

4 *Helmholtz Centre Potsdam, German Research Centre for Geosciences (GFZ), Telegrafenberg, 14473*  
5 *Potsdam (Germany)*

6 \* *rosen@gfz-potsdam.de*

7

8

9 ***Pre-print on earthArXiv***

10

11 Please cite as:

12 Rosenau, M., Rudolf, and Oncken, O. (2019): Creep on seismogenic faults: Insights from analogue  
13 earthquake experiments. SFB1114 Preprint in EarthArXiv. pp. 1-22.  
14 <https://dx.doi.org/10.17605/OSF.IO/--->

15

16

17 **Highlights**

- 18 • Stick-slip experiments mimic seismogenic fault behavior
- 19 • Creep and earthquakes are not mutually exclusive fault styles
- 20 • Interseismic creep varies systematically with fault properties and stress state

21

22

23 **Keywords**

24 *friction, faults, granular materials, aseismic creep, earthquakes, precursors*

25

26 **Abstract**

27 *Tectonic faults display a range of slip behaviors including continuous and episodic*  
28 *slip covering rates of more than 10 orders of magnitude (<mm/a to >m/s). The*  
29 *physical control of such kinematic observations remains ambiguous. To gain insight*  
30 *into the slip behavior of brittle faults we performed laboratory stick-slip experiments*  
31 *using a rock analogue, granular material. We realized conditions under which our*  
32 *seismogenic fault analogue shows a variety of slip behaviors ranging from slow,*  
33 *quasi continuous creep to episodic slow slip to dynamic rupture controlled by a*  
34 *limited number of parameters. We explore a wide parameter space by varying loading*  
35 *rate from those corresponding to interseismic to postseismic rates and normal loads*  
36 *equivalent to hydrostatic to lithostatic conditions at seismogenic depth. The*  
37 *experiments demonstrate that significant interseismic creep and earthquakes may not*  
38 *be mutually exclusive phenomena and that creep signals vary systematically with the*  
39 *fault's seismic potential. Accordingly, the transience of interseismic creep scales with*  
40 *fault strength and seismic coupling as well as with the maturity of the seismic cycle.*  
41 *Loading rate independence of creep signals suggests that mechanical properties of*  
42 *faults (e.g. seismic coupling) can be inferred from shortterm observations (e.g.*  
43 *aftershock sequences). Moreover, we observe the number and size of small episodic*  
44 *slip events to systematically increase towards the end of the seismic cycle providing*  
45 *an observable proxy of the relative shear stress state on seismogenic faults. Modelling*  
46 *the data suggest that for very weak faults in a late stage of their seismic cycle, the*  
47 *observed creep systematics may lead to the chimera of a perennially creeping fault*  
48 *releasing stress by continuous creep and/or transient slow slip instead of large*  
49 *earthquakes.*

50

## 51        **1. Introduction**

52        Faults in the brittle part of the lithosphere may slip at rates ranging from slow,  
53        aseismic ( $< 1 \text{ mm/a}$ ) to fast, seismic ( $> 1\text{m/s}$ ) (Peng and Gomberg, 2010, and  
54        references therein). Moreover they might do so in either continuous (i.e. at constant  
55        rate) or transient fashion (at changing rate). Modern geodetic methods allow  
56        monitoring fault slip rates over time scales long enough to cover a significant part of  
57        the loading history (generally decades) for some fast loading settings like plate  
58        boundaries thereby constraining their kinematic behavior with unprecedented  
59        resolution (Moreno et al., 2010; Shirzaei and Bürgmann, 2013). Accordingly, a suite  
60        of slip behaviors has been observed ranging from continuous creep (e.g., Bokelman  
61        and Kovach, 2003) to transient creep (e.g. precursory and afterslip) (e.g. Bedford et  
62        al., 2013, Schurr et al., 2014) to episodic slip events at various rates (earthquakes,  
63        slow slip and non-volcanic tremor, low frequency earthquakes, creep events) (e.g.  
64        Rogers and Dragert, 2003; Ide et al., 2007). High fluid pressure has been identified as  
65        a controlling factor for slow slip phenomena (e.g., Peng and Gomberg, 2010, Moreno  
66        et al, 2014) but the underlying mechanisms and mechanics controlling which slip  
67        behavior prevails remain under determined. Importantly the physics of such faulting is  
68        often intrinsically undeterminable in nature because of the inaccessibility of the  
69        source and the ambiguity of the geophysical and kinematic observation which can be  
70        fitted by more than one theoretical models and/or set of model parameters.

71        Seismic and aseismic slip behavior are conventionally viewed as mutually exclusive at a  
72        given location through time. Typically “ambivalent” fault slip behaviors are modelled  
73        as a result of the interaction of spatially separated sources, e.g. a seismogenic patch  
74        (asperity) embedded in an aseismic area (barriers) (e.g., Wei et al., 2013). However, a  
75        more integrative view of slow and fast slip phenomena might be possible where the

76 slip behavior is non-unique (e.g. Peng and Gomberg, 2010). Indeed, there is recent  
77 evidence from longterm geodetic observations as well as contrasting geodetic-  
78 seismological versus palaeoseismological observations that given fault areas might be  
79 more variable in their slip behaviors than conventionally believed. In particular we  
80 now have to acknowledge that a particular fault area may show aseismic creep or slow  
81 slip at one time while failing catastrophically in dynamic earthquake ruptures at  
82 others. Examples of spatially overlapping seismic and aseismic fault areas have been  
83 found along the Hayward fault in California U.S. (Lienkaemper et al., 2012, Shirzaei  
84 and Bürgmann, 2013) as well along the subduction megathrusts off Japan (Loveless  
85 and Meade, 2011, Kato et al, 2012) and Chile (Moreno et al, 2010, Ruiz et al, 2014).  
86 As a reaction to such evidence for non-unique slip behavior, existing friction laws  
87 have been adapted for example by allowing aseismic creep at low slip rates but  
88 dynamic weakening at high slip rates, e.g. in the presence of fluids (e.g. Noda and  
89 Lapusta, 2013).

90 We here contribute to the discussion of creep signals by means of experimental  
91 modeling seismogenic fault slip behavior using a lab-scale fault analogue under  
92 conditions relevant to natural faulting. We show that few parameters can control the  
93 rate and stability of fault slip and demonstrate that creeping faults can generate  
94 earthquakes. Showing the systematics by which this happens allows inferring  
95 information on the mechanical properties and state of the fault from kinematic  
96 observations.

## 97 **2. Friction regimes**

98 The most established view on the mechanics of faulting in the brittle regime ( $< c$ .  
99  $350^{\circ}\text{C}$ ) is represented by the rate-and-state dependent friction law (e.g. Scholz, 1998).  
100 This law opens avenues to explain fault slip behavior over a range of rates. In

101 particular, it relates aseismic and seismic fault behavior to an intrinsic velocity-  
102 strengthening and velocity-weakening fault property, respectively. Accordingly, once  
103 static friction is overcome a velocity-weakening fault may weaken dynamically as slip  
104 accelerates resulting in a runaway effect or instability and nucleating an earthquake.  
105 In contrast, an increase of dynamic friction along a velocity strengthening fault  
106 inhibits earthquake nucleation at all times. Importantly, a third regime exists, in which  
107 most of the natural faults might actually be, which is characterized by velocity  
108 weakening under sufficiently low effective normal stress  $\sigma_n'$  (e.g. near the surface or  
109 at high pore fluid pressures). In this regime, which is called the conditionally stable  
110 regime, fault slip is slow and stable under quasi-static loading while it can become  
111 unstable under dynamic loading (acceleration). “Sufficiently” low effective normal  
112 stress in the context of conditional stability means that the externally applied normal  
113 load minus the local pore fluid pressure is below a critical value  $\sigma_c$ :

$$114 \quad \sigma_n' < \sigma_c = kL / -(a-b) \quad (i)$$

115 where  $k$  is the spring stiffness in the original theoretical spring slider framework (or  
116 the stiffness of the medium in which the fault is embedded),  $a$  the instantaneous  
117 change of friction following a loading rate change (so-called direct velocity effect)  
118 and  $b$  the new steady state friction (so-called evolutionary effect) after the loading rate  
119 change which evolves over the characteristic slip distance  $L$  (a physical interpretation  
120 is the size of asperities). The combined parameter  $a-b$  is negative for velocity  
121 weakening interfaces and positive for velocity-strengthening interfaces. Its absolute  
122 values are typically measured in the lab to be in the order of few percent for rocks and  
123 other materials (Scholz, 1998; and references therein).

124

### 125 3. Analogue earthquake experimental setup

126 The laboratory-scale analogue earthquake experiments presented here have been  
127 performed in a ring shear tester setup (RST, Figure 1) where a granular material (dry  
128 rice) is sheared rotary in a velocity stepping test under imposed normal loads while  
129 shear stress is measured continuously. The rate of laboratory fault slip has been  
130 inferred from displacement records derived by particle image velocimetry (PIV,  
131 LaVision Strainmaster ®). For PIV analysis, a 12 bit monochrome charged-coupled  
132 device (CCD) camera shot sequential images of the analogue fault through a  
133 transparent shear cell at a frequency of 10 Hz. The particle motions between  
134 successive images are then determined by cross-correlation of textural differences  
135 (i.e., gray values) formed by groups of particles within interrogation windows using a  
136 Fast Fourier Transform algorithm (Adam et al. 2003). Precision and accuracy of the  
137 PIV method is better than 0.1 px of the original image which scales to the order of  
138 micrometer in the presented setup.

139 The stiffness of the loading system ( $\sim 1.3$  kN/mm) together with  $a$ - $b$  ( $\sim -0.015$ ) and  $L$   
140 ( $\sim 2$   $\mu\text{m}$ ) for dry rice (Rosenau et al., 2009) predicts a critical (effective) normal stress  
141 of  $\sigma_c = 8$  kPa. Accordingly, we performed the tests at 1 – 16 kPa normal load to  
142 explore the slip behavior of natural faults across the bifurcation. We refer to the high  
143 (8, 16 kPa) and low (1, 2, 4 kPa) normal stress experiments as strong and weak faults,  
144 respectively.

145 Similarity of the experimental simulation with its natural prototype is ensured by  
146 keeping the following dimensionless numbers the same: (1) the friction coefficient  
147 (ratio between yield strength and normal stress)  $\mu \sim 0.7$ , (Byerlee, 1978) and (2) a  
148 friction rate parameter  $a$ - $b \sim -0.015$  similar to rocks (e.g., Scholz, 1998) as well as (3)

149 a dimensionless stress drop (ratio between rupture slip and length) of  $\Delta\tau^* \sim 10^{-5} - 10^{-4}$   
150 similar to earthquakes (e.g., Scholz, 1989).

151 Applying a stress scale of 1:10.000, the setup generates slip instabilities (aka  
152 “analogue earthquakes”, Figure 2) with stress drops which scale to 1 – 100 MPa in  
153 nature typical of large intra- and interplate earthquakes (Scholz, 1989; Hardebeck and  
154 Aron, 2009) including precursory events of different scale (Figure 3). The strength of  
155 the laboratory fault analogues can be interpreted in two way: Either representing (A)  
156 different crustal depths at a given pore fluid pressure (i.e. weak = shallow, strong =  
157 deep) or (B) representing different pore fluid pressures at a given depth. For example,  
158 at typical seismogenic crustal depths of 5 – 15 km and typical rock densities of 2300 –  
159 2700 kg/m<sup>3</sup>, the experimental normal stresses (10 – 160 MPa) would correspond to  
160 pore fluid pressures of 38 – 96 % lithostatic pressure, i.e. from hydrostatic to near  
161 lithostatic. Time is not explicitly scaled in the experiments but imposed loading rates  
162 cover more than two orders of magnitude (0.1 – 25 mm/min) similar to post- and  
163 interseismic deformation rates in nature (mm/day – mm/year) in order to test possible  
164 time scale dependencies (or independencies) of creep signals.

#### 165 **4. Experimental observations and analysis**

166 Analogue fault slip in our experiments is characterized by quasi-periodic stress drops  
167 (Figure 2). Quasi-periodic stress drops are preceded by smaller, episodic events  
168 (Figure 3). The sizes and recurrence intervals of periodic stress drops are  
169 systematically related to the applied normal load and loading rate (Figure 4). This  
170 observation is consistent with normal load and loading rate both determining the yield  
171 strength according to rate-and-state friction theory (Scholz, 1998). A regular stick-slip  
172 behavior is consistent with a characteristic earthquake model where episodic slip  
173 occurs at a certain stress level determined by the yield strength and causes relaxation



174 to a certain lower stress level determined by the residual friction and the stiffness of  
175 the loading system.

176 Beside periodic and episodic stress drops, representing slip during earthquakes and  
177 slow slip events, a significant amount of long-term laboratory fault slip occurs as  
178 transient creep (accelerating stable slip) between episodic failures. This stable slip  
179 during the “stick”-phase causes the stress curves in Figures 2 and 3 to deviate from a  
180 linear, elastic loading path. Instead of an ideal “saw tooth” pattern characterizing  
181 stress histories of perfect stick-slip, a “shark fin” pattern emerges for the observed  
182 stick-creep-slip. In the experiments, up to 80 % of long-term fault slip might be taken  
183 up by creep at low effective normal stresses resulting in seismic coupling coefficients  
184 (the ratio of seismic to total fault slip) of  $<0.2$  for very weak faults (Figure 2C). At  
185 high normal stresses, seismic coupling increases to  $>0.8$  for strong faults in the  
186 experiments.

187 Detailed inspection of the stress loading paths (Figure 5 A) and interseismic creep  
188 signals (Figure 5 B) and their time-derivates (i.e. loading and slip rates, Figure 5 C  
189 and D) sheds light on the time and stress dependencies of laboratory fault creep.

190 Accordingly, stress in the inter-event time (which is normalized to a unit interval  
191 here) accumulates in a more transient, non-linear fashion for weak faults than it does  
192 for strong faults (red versus blue curves in Figure 5 A and C). Strong faults show a  
193 stressing rate which is almost consistent with elastic loading except prior to an event  
194 (i.e. runs parallel long-term rate in Figure 5 C) while stressing rates of weak faults  
195 vary by more than an order of magnitude. Slip varies consistently with loading.

196 Accordingly, slip accumulates in a more non-linear for strong faults than it does for  
197 weak faults (Figure 5 B) covering two orders of magnitude in slip rate versus less than  
198 one, respectively (Figure 5 D).

199 Connecting stress and strain allow us to describe the creep behavior of our fault  
200 analogues as follows: Creep along strong laboratory faults accelerates at rather  
201 constant stressing rate late in the interseismic period leading to episodic failure  
202 (“precursory slip”). Weak faults instead creep at higher rates throughout the  
203 interseismic period but more continuously and at progressively decreasing stressing  
204 rate. Moreover, strong faults reach only about half of the long-term fault slip rate  
205 towards the very end of the loading cycle, whereas weak faults may creep at almost  
206 the long-term rate for the second half of the loading cycle.

207 In order to analyze the creep behavior systematically as controlled by extrinsic factors  
208 (normal stress and loading rate) we attempted to quantify the non-linearity (or  
209 transience) of stress and slip accumulation by a single, dimensionless parameter.  
210 Therefore we calculated the area beneath the normalized stress and strain  
211 accumulation curves in Figure 5 A and B, respectively, which we call the unit stress  
212 and unit strain integrals (Figure 5E). Clearly, these measures of transience decrease  
213 systematically with increasing applied normal stress or fault strength as expected from  
214 the observations before. However, they do not correlate with loading rate, an  
215 observation that is not intuitive but useful as will be discussed below. The positive  
216 correlation between the unit stress and slip integrals (Figure 5F) indicates the  
217 consistency of our independent stress and strain observations and is a direct result of  
218 the intrinsic velocity weakening behavior of the laboratory fault.

219 Irrespective of fault strength, episodic slip events of various speeds occur at high  
220 stress level modulating the interseismic creep signal in the late stage of the analogue  
221 seismic cycle (Figure 3). Preliminary analysis suggests that these precursor events  
222 increase systematically in number and size as the fault evolves towards failure.

223

224 **5. Discussion**

225 **5.1 Inversion of fault properties and state from creep signals**

226 The observation of continuous and transient creep signals as well as episodic slow  
227 slips which are systematically linked to fault properties and maturity of the loading  
228 cycle or stress level but independent of loading rate bear important implications for  
229 the interpretation of fault creep records as observable proxies for fault strength and  
230 seismic potential. Fault creep records in nature are generally short with respect to the  
231 seismic cycle. The results obtained here suggest that any creep record, though only a  
232 snapshot of the full seismic cycle, might bear important information on long-term  
233 fault properties and hazardous behavior.

234 Using the analog fault observations from the here presented experiments, an empirical  
235 inversion scheme as proposed in Figure 6 can be applied, where inaccessible fault  
236 properties like fault strength, seismic coupling, stress drop and recurrence interval can  
237 be inferred from the observable transience of interseismic creep signals. Here, creep  
238 transience (CT) is defined as

239 
$$CT = 2 \cdot (1 - 2 \cdot \text{unit slip integral}) \quad (\text{ii})$$

240 in order to derive a dimensionless (and therefore scale-independent) parameter which  
241 varies between 0 (linear strain accumulation) and 1 (non-linear, highly transient strain  
242 accumulation).

243 Linear regression analysis of the experimentally derived data plotted in such a scheme  
244 indicates a significant correlation between creep signals and fault properties and  
245 behavior but independence of loading rate. More specifically, fault strength, seismic  
246 coupling, stress drop as well as recurrence period show a positive linear or log-linear  
247 dependency with CT ( $R^2 > 0.6 - 0.8$ ).

248 Importantly, no significant correlations exist between any of the parameters with  
249 loading rate. This is indicated by the rather horizontal or scattered distribution of data  
250 from subsets with the same fault strength measured at different velocities in Figure 6  
251 as well as the collapse of time-series data from such subsets in Figure 5. The fact that  
252 the systematics found experimentally are loading rate independent suggest that short-  
253 term observations can be extrapolated to larger earthquakes and longer recurrence  
254 intervals. I.e. this timescale independency opens the opportunity to generalize fault  
255 properties or behavior derived during aftershocks sequences or earthquake swarms or  
256 from repeating events to longterm (multiple seismic cycles) fault behavior.

257 An observation not quantified in detail here is the occurrence of precursor slip events  
258 of different scale and velocity which systematically increase in number and size  
259 towards the end of a seismic cycle (Figure 3). Several large earthquakes in subduction  
260 zones have actually been preceded by accelerating foreshock activity (e.g. Bouchon et  
261 al., 2013). Especially the recent 2014 8.1 Pisagua earthquake offshore Chile showed  
262 accelerating foreshock activity with a decrease in b-value (representing an increase in  
263 the number of large events relative to small events) over the decade preceding the  
264 main shock (Schurr et al., 2014). If such a systematic behavior can be generalized and  
265 physically explained it should lead to a better ability to forecast earthquakes.

## 266 **5.2 Revisiting creep records along the San Andreas Fault**

267 In order to test and apply our proposed inversion scheme, we use the longest creep  
268 records available and revisit the San Andreas Fault data. California creepmeters have  
269 been installed across the San Andreas Fault in the late 1960s (Schulz et al., 1982),  
270 geodetic surveys took place since the mid-1970s (Burford and Harsh, 1980; Lisowski  
271 and Prescott, 1981) and surface velocities from space-geodetic measurements are  
272 available since about a decade (e.g., Bürgmann et al., 2000; Titus et al., 2006). For a

273 mean recurrence interval of large Californian earthquakes of about  $150 \pm 50$  years  
274 along any SAF segment (e.g. Zielke et al., 2010), the observation time frame  
275 generally represents less than half of the seismic cycle length. Nevertheless, the  
276 records are probably the best data we can get today.

277 Seismic and aseismic strike-slip along the central SAF (cSAF) accounts for most of  
278 the Pacific-Great Valley microplate relative motion in central California (Thatcher,  
279 1979; Lisowski and Prescott, 1981, Titus et al., 2006; Rolandone et al., 2008; Ryder  
280 and Bürgmann, 2008). As suggested by over 40 years of creep and earthquake  
281 records, the central section of the cSAF creeps continuously at a decadal scale at  
282 about 28 mm/a at seismogenic depth (0 – 12 km, Schulz et al., 1982, Titus et al.,  
283 2006, Rolandone et al., 2008). This long-term creep is modulated by shorter term  
284 transients presumably very shallow (< 5 km) and related to earthquakes (Lisowski and  
285 Prescott, 1981; Thurber, 1996). At seismogenic depths repeating microearthquakes  
286 occur (Nadeau and McEvilly, 2004) indicating that locally and/or transiently, velocity  
287 weakening behavior is established along the fault. Noticeably, the current creep of  
288 cSAF is only about 80 – 90 % of the far-field, tectonic loading rate (31 – 35 mm/a,  
289 Titus et al., 2006, Rolandone et al., 2008; Ryder and Bürgmann, 2008) suggesting a  
290 slip deficit of few millimeter accumulating each year. Right-lateral shear strains in the  
291 sidewalls of the cSAF are evidently very small (Rolandone et al., 2008, Savage, 2009)  
292 suggesting a small stressing rate. Episodic slow slip events as they occur late in the  
293 interseismic period in our experiments (Figure 3) have been reported as potential  
294 earthquake pre-cursors along the SAF by Thurber (1996) and Thurber and Sessions  
295 (1998) based on temporal cross-correlation of creepmeter records and seismological  
296 catalogues. Though the correlations they found were statistically significant, the  
297 feedback mechanism remained unclear. Noticeably, they did not find a clear spatial

298 relation between the loci of creep and earthquakes which would be required by our  
299 model. Moreover, they assigned creep to the very shallow crust (<5 km) and not to  
300 seimogenic depths. Whilst the adjoining segments ruptured in large earthquakes in  
301 1906 (San Francisco) and 1857 (Fort Tejon), the creeping section of the cSAF has not  
302 experienced large earthquakes in the historic past (~300 years).

303 In the light of the experiments done in this study the key question is: Does the absence  
304 of large earthquakes, the high and continuous creep rates as well as the low shear  
305 strain accumulation serves as a good indicator that this fault segment poses no seismic  
306 hazard?

307 Applying the empirical inversion scheme established above (Figure 6), we would  
308 infer first that the creeping section of the cSAF is a very weak fault based on the  
309 rather linear slip accumulation signal (Schulz et al., 1982, Titus et al., 2006) and low  
310 stressing rate (Rolandone et al., 2008, Savage, 2009). This is consistent with previous  
311 findings based on the observation of low resolved shear stresses along the creeping  
312 section and absence of a heat flow anomaly (Brune et al., 1969, Lachenbruch and  
313 Sass, 1980, Zoback et al., 1987).

314 The cSAF shows therefore kinematic similarity to our weak fault analogue  
315 characterized dynamically by low seismic coupling and small stress drops during  
316 earthquakes. This may however not mean that the seismic potential is low. In contrast:  
317 Because stress drop is only a weak measure of earthquake size, which scales  
318 dominantly with the rupture area, and because low seismic coupling (or vice versa a  
319 large amount of interseismic creep) just stretches the recurrence intervals of  
320 potentially large earthquakes. We will elaborate on this effect in the next section.

321 **5.3 Modelling the effect of creep on recurrence time and the chimera of**  
322 **perennially creeping faults**

323 Because of the empirically found correlation between fault strength and creep, the net  
324 effect of creep on the recurrence interval of earthquakes should not only take into  
325 account the stretching of the recurrence interval due to creep but also a modification  
326 of recurrence interval due to changes in strengths (Figure 4). Such a scenario is  
327 illustrated in Figure 7.

328 Quantitatively, creep lengthens the (effective) recurrence interval to

329 
$$t^* = 1/(1-\text{creep}). \quad (\text{iii})$$

330 For example a fault where 50 % of longterm slip is accommodated aseismically  
331 requires twice as much time to reach a certain stress level again. However, because  
332 creep correlates with fault weakness and weaker faults fail at lower stress level in  
333 quicker succession for the same far field stressing rate (Figure 4), this lengthening  
334 effect is to some degree counterbalanced by shorter recurrence intervals.

335 In Figure 7 we plot the effective recurrence time observed in our experiments in  
336 relation to creep on faults of variable strength and model the data as the combined  
337 result of the competing effects of “creep lengthening” (according to eq. (iii)) and  
338 “weakness shortening”. The latter effect is taken into account by fitting an  
339 exponential relation of the form

340 
$$t^{**} = e^{(-A \times \text{creep})} \quad (\text{iv})$$

341 to the data. Parameter  $A$  is an empirically derived proxy for the relation between  
342 strength and recurrence interval and varies between 4 and 6 in our example. The net  
343 effect of “creep lengthening” and “weakness shortening” of recurrence intervals, i.e.  
344 the effective recurrence interval, is then simply

345 
$$t = t^* \times t^{**} = 1/(1-\text{creep}) e^{(-A \times \text{creep})}. \quad (\text{v})$$

346 For the parameter space realized in our experiments recurrence time is always shorter  
347 than on faults without creep, i.e. the weakness effect dominates the recurrence  
348 behavior such that more creeping faults have systematically shorter recurrence times.  
349 However, at least theoretically our model predicts for very weak faults (not realized in  
350 our experiments) with very low seismic coupling coefficients and very high creep  
351 amounts, the lengthening effect should start dominating and consequently the  
352 effective recurrence intervals should become longer than without creep. For creep  
353 amounts exceeding 98% effective recurrence times may well exceed any historical  
354 record for fast creeping faults (Figure 7). In the extreme such a seismically nearly  
355 uncoupled, very weak fault appears as seismically silent over many human  
356 generations – obviously a chimera.

#### 357 **5.4 Creep on continental vs. subduction megathrusts**

358 Locking pattern of continental and subduction megathrusts show a striking qualitative  
359 difference: While continental megathrusts, e.g. the Himalayan main thrust, show  
360 homogeneous and high locking with little interseismic creep (Stevens and Avouac,  
361 2015), subduction megathrusts, like the Chilean subduction zone, show a patchy  
362 locking pattern indicating a significant amount of creep (e.g. Saillard et al., 2017).  
363 According to our experiments, and in line with theory, such a qualitative difference  
364 can be explained by higher amounts water entrained into subduction megathrust  
365 compared to continental settings, lowering the effective normal load and this  
366 enhancing creep. However, other explanations exist like differences in lithology and  
367 even lack of offshore geodetic coverage.

368



369 **6 Conclusion**

370 Based on stick-slip experiments using a lab-scale fault analogue, we explored the slip  
371 behavior of seismogenic faults and tested the potential to derive information on fault  
372 properties and state from kinematic observables. We showed that the stress buildup  
373 between episodic failures (analogue earthquakes) is non-linear and anti-correlated  
374 with the creep signals. According to our experiments the transience of stress buildup  
375 and creep is controlled primarily by fault normal stress, i.e. related to frictional  
376 strength and/or pore-fluid pressure, and systematically reflect the seismic coupling  
377 coefficient and maturity of the seismic cycle. Application of these systematics to the  
378 creeping section of the central San Andreas fault suggests that this fault branch may  
379 not be aseismic on the long term (millennia scale) but is in a late stage of a seismic  
380 cycle which exceeds historic records. The qualitative difference in creep on  
381 megathrusts between homogeneously fully locked continental versus heterogeneously  
382 locked subduction megathrusts may be similarly explained by the presence of water in  
383 oceanic settings.

384 **Acknowledgements**

385 This study has been partially funded by the German Research Foundation (DFG)  
386 collaborative research center SFB1114 “Scaling Cascades in Complex Systems”,  
387 project B01.

388

389 **Figure Captions**

390 **Figure 1:** Analogue earthquake experimental setup: (A) side (camera) view of the  
391 sample (rice) in a transparent shear cell in situ in the ring-shear tester, boundary  
392 conditions and observables indicated; PIV velocities are representative of a slip event.  
393 (B) sketch of the ring-shear tester setup (modified from Schulze (2003)) with PIV  
394 camera position indicated.

395 **Figure 2:** Stress and strain time-series of laboratory faults: (A) Stress time series  
396 measured during velocity stepping tests under variable normal loads simulating  
397 seismic and aseismic slip along very weak to strong fault slip. Note the periodic stress  
398 drops representing analogue earthquakes. (B) Slip time series for very weak and  
399 strong faults derived by PIV. (C) Variation of seismic coupling over the parameter  
400 space tested here. Note the sensitivity of seismic coupling to normal load and  
401 insensitivity to loading rate.

402 **Figure 3:** Examples of precursory slip events along laboratory faults: (A) stress time  
403 series, (B) Histogram of number of slow slip events per unit interseismic time  
404 interval. Note the increase of precursory events in size and number towards the end of  
405 the seismic cycle.

406 **Figure 4:** Dependency of recurrence interval and stress drop on loading rate and  
407 normal load over the parameters space tested here.

408 **Figure 5:** Systematics of interseismic stress-strain relationships for laboratory faults:  
409 (A) interseismic stress accumulation (normalized), (B) interseismic slip accumulation  
410 (normalized), (C) interseismic stress rate (normalized), (D) interseismic slip rate  
411 (normalized), (E) Variation of unit stress and slip integrals over the parameter space

412 tested here, (F) correlation of unit stress and slip integrals indicating velocity  
413 weakening behaviour.

414 **Figure 6:** Dependency of creep signal transience on laboratory fault properties: (A)  
415 fault strength as a function of creep transience, (B) seismic coupling as a function of  
416 creep transience, (C) stress drop as a function of creep transience, (D) recurrence  
417 period as a function of creep transience.

418 **Figure 7:** Modelling the effect of fault creep and strength on recurrence time of  
419 earthquakes. Experimental data are fitted by theoretical model taking into account two  
420 competing effect: Fault creep lengthens recurrence intervals (“creep lengthening  
421 effect”) while weakening faults should shorten recurrence intervals (“weakness  
422 shortening effect”). The effective recurrence is dominated by the weakness effect for  
423 faults creeping up to 98%. However, faults which accumulate >98 % of fault slip  
424 aseismically may still generate earthquakes with recurrence periods exceeding  
425 historical records (California earthquake history shown as example).

426

427 **References:**

- 428 1. Adam, J., O. Oncken, N. Kukowski, J. Lohrmann, S. Hoth, J. L. Urai, W. van  
429 der Zee, J. Schmatz, B. Wieneke, and K. Pfeiffer (2005), Shear localisation  
430 and strain distribution during tectonic faulting - New insights from granular-  
431 flow experiments and high-resolution optical image correlation  
432 techniques, *Journal of Structural Geology*, 27(2), 183-301.
- 433 2. Bedford, J., et al. (2013), A high-resolution, time-variable afterslip model for  
434 the 2010 Maule Mw=8.8, Chile megathrust earthquake, *Earth and Planetary  
435 Science Letters*, 383, 26-36.
- 436 3. Bokelmann, G. H. R. (2003), Long-term creep-rate changes and their  
437 causes, *Geophysical Research Letters*, 30(8).
- 438 4. Bouchon, M., V. Durand, D. Marsan, H. Karabulut, and J. Schmittbuhl (2013),  
439 The long precursory phase of most large interplate earthquakes, *Nature  
440 Geoscience*, 6(4), 299-302.
- 441 5. Brune, J. N., T. L. Henyey, and R. F. Roy (1969), Heat flow, stress, and rate of  
442 slip along the San Andreas Fault, California, *Journal of Geophysical  
443 Research*, 74(15), 3821--3827.
- 444 6. Burford, R. O., and P. W. Harsh (1980), Slip on the San Andreas fault in  
445 central California from alignment array surveys, *Bulletin of the Seismological  
446 Society of America*, 70(4), 1233-1261.
- 447 7. Byerlee, J. (1978), Friction of rocks, *Pageoph*, 116, 615-626.
- 448 8. Bürgmann, R., D. Schmidt, R. M. Nadeau, M. d'Alessio, E. Fielding, D.  
449 Manaker, T. V. McEvilly, and M. H. Murray (2000), Earthquake Potential

- 450 Along the Northern Hayward Fault, California, *Science*, 289(5482), 1178-  
451 1182.
- 452 9. Hardebeck, J. L., and A. Aron (2009), Earthquake Stress Drops and Inferred  
453 Fault Strength on the Hayward Fault, East San Francisco Bay,  
454 California, *Bulletin of the Seismological Society of America*, 99(3), 1801-  
455 1814.
- 456 10. Ide, S., G. C. Beroza, D. R. Shelly, and T. Uchide (2007), A scaling law for  
457 slow earthquakes, *Nature*, 447(7140), 76-79.
- 458 11. Kato, A., K. Obara, T. Igarashi, H. Tsuruoka, S. Nakagawa, and N. Hirata  
459 (2012), Propagation of Slow Slip Leading Up to the 2011 M-w 9.0 Tohoku-  
460 Oki Earthquake, *Science*, 335(6069), 705-708.
- 461 12. Lachenbruch, A. H., and J. H. Sass (1980), Heat flow and energetics of the  
462 San Andreas Fault Zone, *Journal of Geophysical Research: Solid*  
463 *Earth*, 85(B11), 6185--6222.
- 464 13. Lienkaemper, J. J., J. N. Baldwin, R. Turner, R. R. Sickler, and J. Brown  
465 (2013), A Record of Large Earthquakes during the Past Two Millennia on the  
466 Southern Green Valley Fault, California, *Bulletin of the Seismological Society*  
467 *of America*, 103(4), 2386-2403.
- 468 14. Lisowski, M., and W. H. Prescott (1981), Short-range distance measurements  
469 along the San Andreas fault system in central California, 1975 to  
470 1979, *Bulletin of the Seismological Society of America*, 71(5), 1607-1624.
- 471 15. Loveless, J. P., and B. J. Meade (2011), Spatial correlation of interseismic  
472 coupling and coseismic rupture extent of the 2011 MW= 9.0 Tohoku-oki  
473 earthquake, *Geophysical Research Letters*, 38(17).

- 474 16. Moreno, M., M. Rosenau, and O. Oncken (2010), 2010 Maule earthquake slip  
475 correlates with pre-seismic locking of Andean subduction  
476 zone, *Nature*, 467(7312), 198-202.
- 477 17. Moreno, M., C. Haberland, O. Oncken, A. Rietbrock, S. Angiboust, and O.  
478 Heidbach (2014), Locking of the Chile subduction zone controlled by fluid  
479 pressure before the 2010 earthquake, *Nature Geoscience*, 7(4), 292-296.
- 480 18. Nadeau, R. M., and T. V. McEvilly (2004), Periodic Pulsing of Characteristic  
481 Microearthquakes on the San Andreas Fault, *Science*, 303(5655), 220-222.
- 482 19. Noda, H., and N. Lapusta (2013), Stable creeping fault segments can become  
483 destructive as a result of dynamic weakening, *Nature*, 493(7433), 518-+.
- 484 20. Peng, Z. G., and J. Gomberg (2010), An integrated perspective of the  
485 continuum between earthquakes and slow-slip phenomena, *Nature*  
486 *Geoscience*, 3(9), 599-607.
- 487 21. Rogers, G., and H. Dragert (2003), Episodic tremor and slip on the Cascadia  
488 subduction zone: The chatter of silent slip, *Science*, 300, 1942-1943.
- 489 22. Rolandone, F., R. Bürgmann, D. C. Agnew, I. A. Johanson, D. C. Templeton,  
490 M. A. d'Alessio, S. J. Titus, C. DeMets, and B. Tikoff (2008), Aseismic slip  
491 and fault-normal strain along the central creeping section of the San Andreas  
492 fault, *Geophysical Research Letters*, 35(14), n/a--n/a.
- 493 23. Rosenau, M., J. Lohrmann, and O. Oncken (2009), Shocks in a box: An  
494 analogue model of subduction earthquake cycles with application to  
495 seismotectonic forearc evolution, *Journal of Geophysical Research*, 114(B1).

- 496 24. Ruiz, S., M. Metois, A. Fuenzalida, J. Ruiz, F. Leyton, R. Grandin, C. Vigny,  
497 R. Madariaga, and J. Campos (2014), Intense foreshocks and a slow slip event  
498 preceded the 2014 Iquique Mw 8.1 earthquake, *Science*.
- 499 25. Ryder, I., and R. Bürgmann (2008), Spatial variations in slip deficit on the  
500 central San Andreas Fault from InSAR, *Geophysical Journal  
501 International*, 175(3), 837--852.
- 502 26. Saillard, M., L. Audin, B. Rousset, J. P. Avouac, M. Chlieh, S. R. Hall, L.  
503 Husson, and D. L. Farber (2017), From the seismic cycle to long-term  
504 deformation: linking seismic coupling and Quaternary coastal geomorphology  
505 along the Andean megathrust, *Tectonics*, 36(2), 241-256.
- 506 27. Savage, J. C. (2009), Comment on “Aseismic slip and fault-normal strain  
507 along creeping section of the San Andreas Fault” by F. Rolandone et  
508 al., *Geophysical Research Letters*, 36(13), n/a--n/a.
- 509 28. Scholz, C. H. (1989), Mechanics of Faulting, *Ann. Rev. Earth Planet. Sci.*, 17,  
510 309-334.
- 511 29. Scholz, C. H. (1998), Earthquakes and friction laws, *Nature*, 391, 37-42.
- 512 30. Schulze, D. (2003), Time- and velocity-dependent properties of powders  
513 effecting slip-stick oscillations, *Chemical Engineering & Technology*, 26(10),  
514 1047-1051.
- 515 31. Schurr, B., et al. (2014), Gradual unlocking of plate boundary controlled  
516 initiation of the 2014 Iquique earthquake, *Nature*, 512(7514), 299-+.
- 517 32. Shirzaei, M., and R. Bürgmann (2013), Time-dependent model of creep on  
518 the Hayward fault from joint inversion of 18 years of InSAR and surface creep  
519 data, *Journal of Geophysical Research-Solid Earth*, 118(4), 1733-1746.

- 520 33. Stevens, V.L., Avouac, J.-P. (2015), Interseismic coupling on the main  
521 Himalayan thrust. *Geophysical Research Letters*, doi:10.1002/2015GL064845
- 522 34. Thatcher, W. (1979), Horizontal crustal deformation from historic geodetic  
523 measurements in southern California, *Journal of Geophysical Research: Solid*  
524 *Earth*, 84(B5), 2351--2370.
- 525 35. Thurber, C. H. (1996), Creep events preceding small to moderate earthquakes  
526 on the San Andreas fault, *Nature*, 380, 425 - 428.
- 527 36. Titus, S. J., C. DeMets, and B. Tikoff (2006), Thirty-Five-Year Creep Rates  
528 for the Creeping Segment of the San Andreas Fault and the Effects of the 2004  
529 Parkfield Earthquake: Constraints from Alignment Arrays, Continuous Global  
530 Positioning System, and Creepmeters, *Bulletin of the Seismological Society of*  
531 *America*, 96(4B), S250-S268.
- 532 37. Wei, M., Y. Kaneko, Y. J. Liu, and J. J. McGuire (2013), Episodic fault creep  
533 events in California controlled by shallow frictional heterogeneity, *Nature*  
534 *Geoscience*, 6(7), 566-570.
- 535 38. Zielke, O., J. R. Arrowsmith, L. G. Ludwig, and S. O. Akçiz (2010), Slip in  
536 the 1857 and Earlier Large Earthquakes Along the Carrizo Plain, San Andreas  
537 Fault, *Science*, 327(5969), 1119-1122.
- 538 39. Zoback, M. D., et al. (1987), New Evidence on the State of Stress of the San  
539 Andreas Fault System, *Science*, 238(4830), 1105-1111.



Figure 1

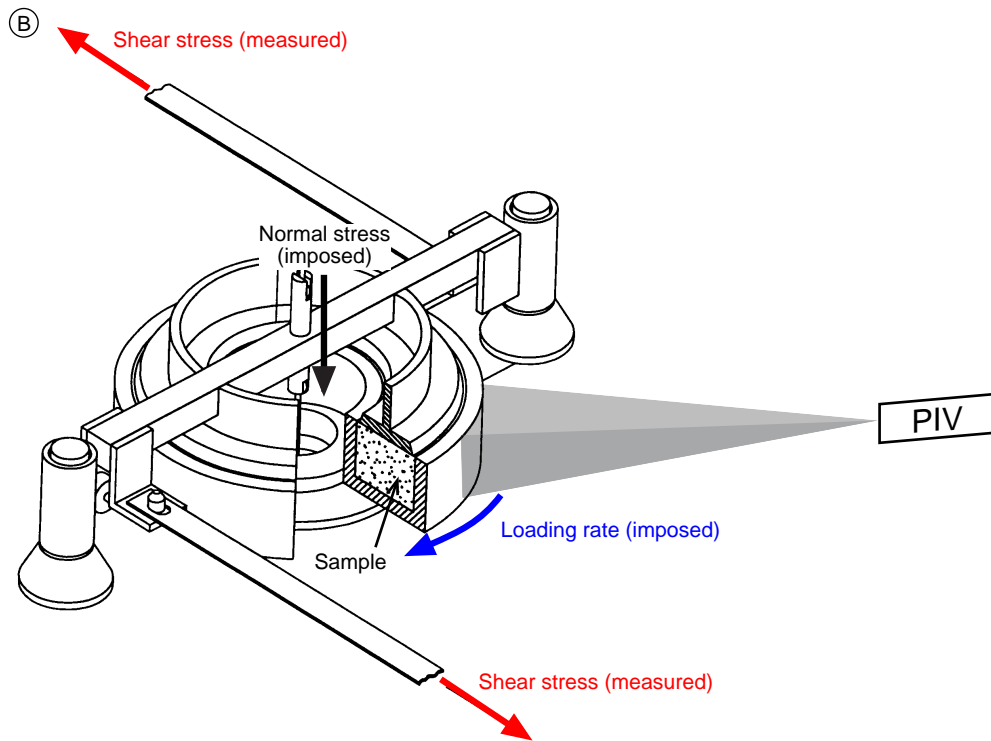
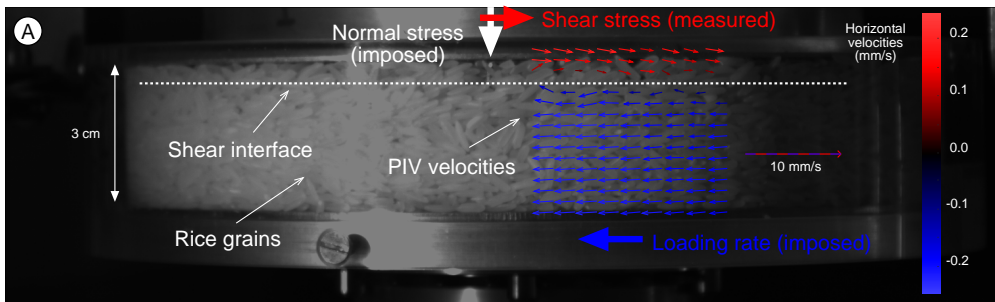


Figure 2

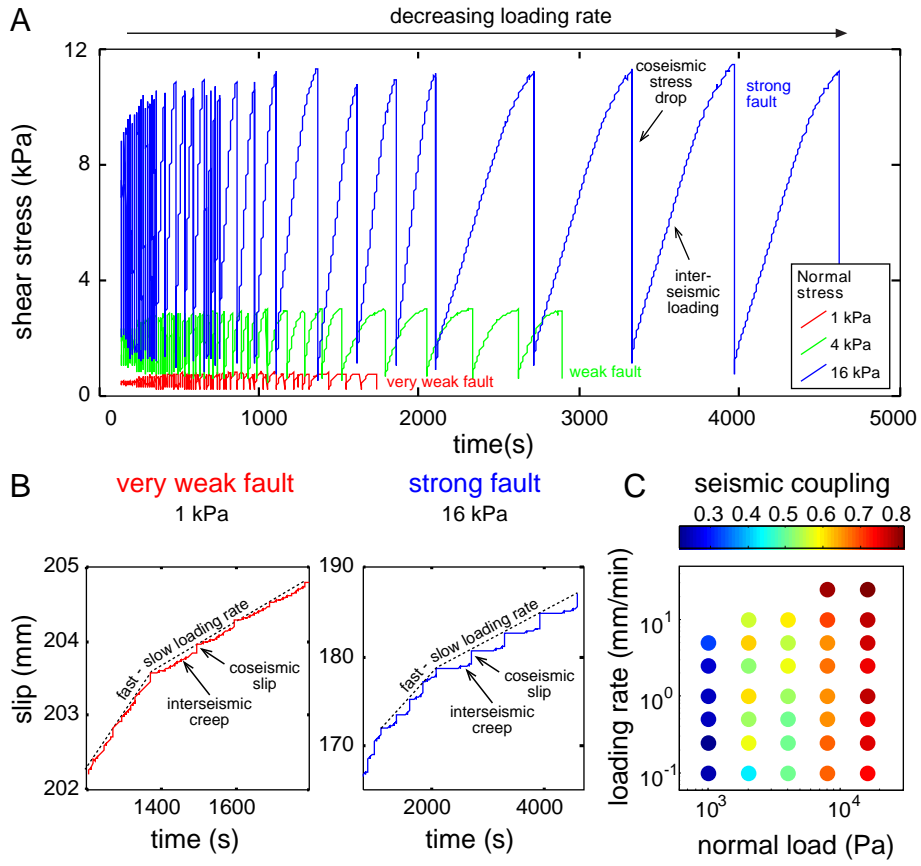


Figure 3

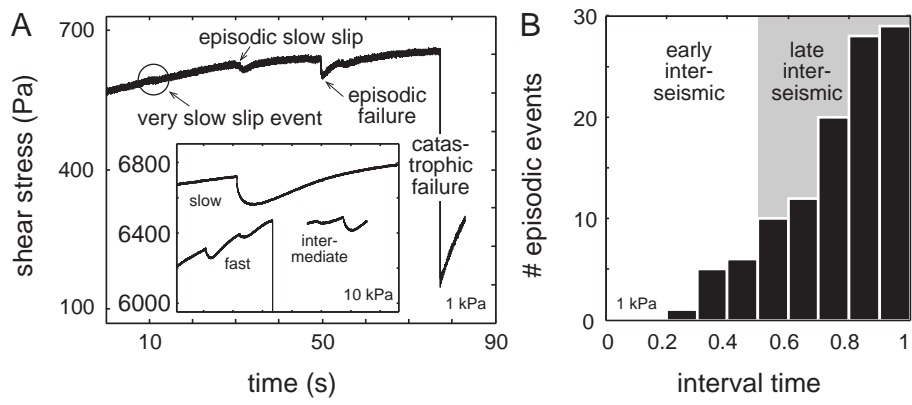


Figure 4

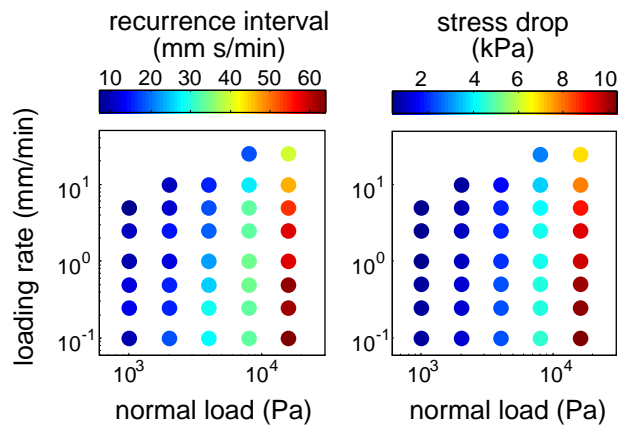


Figure 5

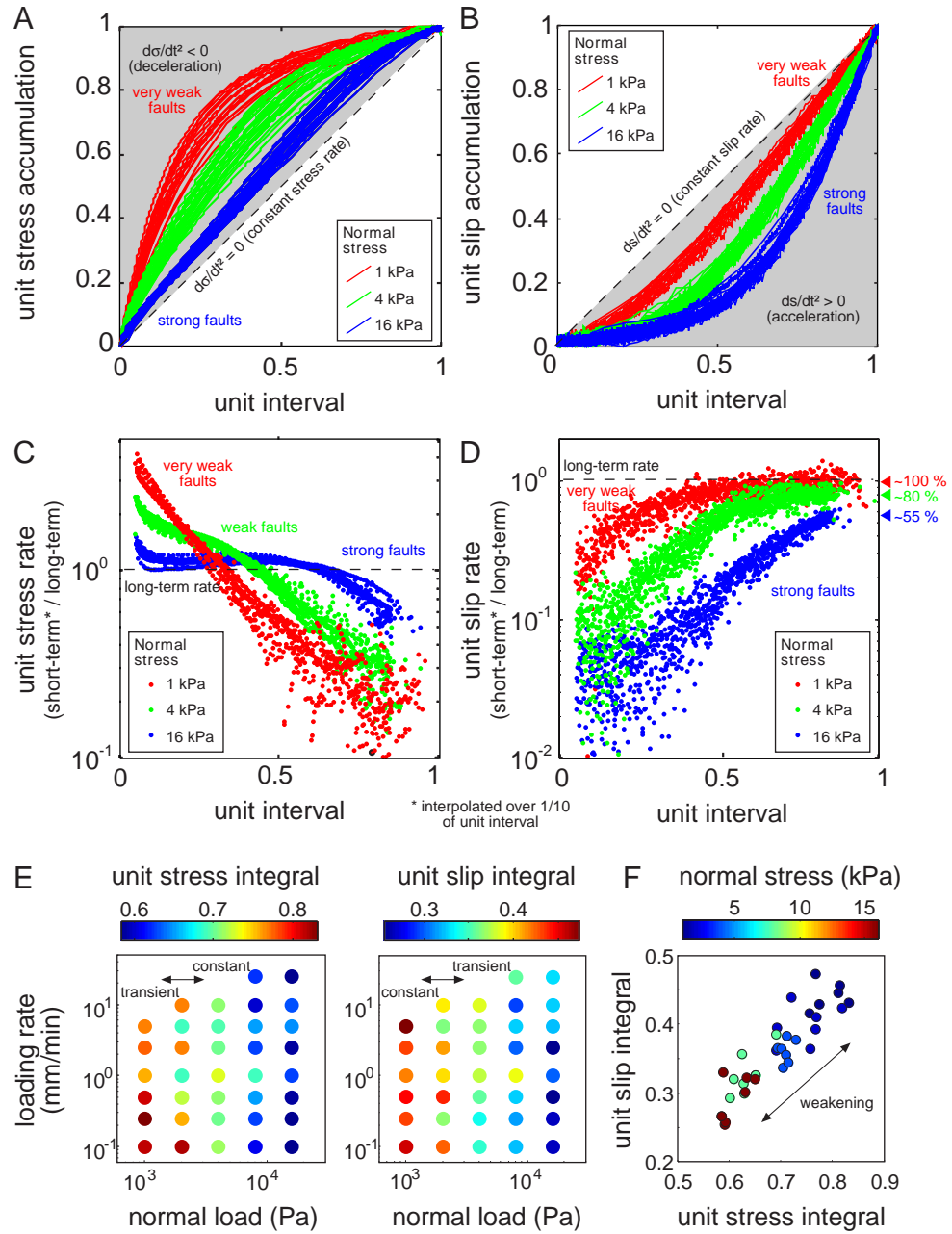


Figure 6

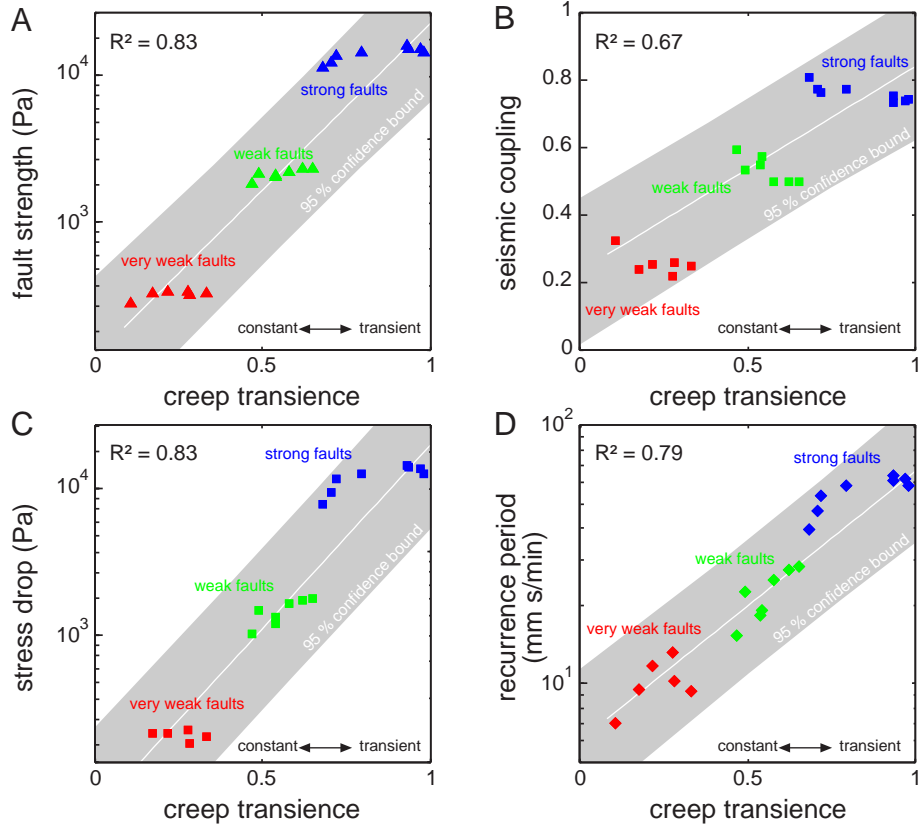


Figure 7

